Dispersion of pressure at the inner edge of the neutron star crust

Ilona Bednarek *
Institute of Physics, University of Silesia, 75 Pułku Piechoty 1, 41-500 Chorzów, Poland

Wiesław Olchawa
Institute of Physics, University of Opole, Oleska 48, 45-052 Opole, Poland

Jan Sładkowski and Jacek Syska
Institute of Physics, University of Silesia, 75 Pułku Piechoty 1, 41-500 Chorzów, Poland

(Received 7 May 2021; revised 19 July 2021; accepted 24 August 2021; published 10 September 2021)

This paper presents a method for estimating the pressure variance at the inner edge of a neutron star crust. The obtained results quantify uncertainty in the estimation of pressure at the core-crust interface, implying that they depend on the selected equation of state and the neutron star's mass distribution function. The quality of the transition pressure determination depends on the neutron star's mass, with a significant decrease in accuracy for configurations with masses close to $2M_\odot$. The method used makes it possible to control the theoretical part of the core-crust pressure dispersion in determining the observational quantities.

DOI: 10.1103/PhysRevC.104.035802

I. INTRODUCTION

Einstein's equations for static spherically symmetric star lead to the relativistic form of hydrostatic equilibrium equations, the solution of which requires supplementing with the equation of state (EoS) and allows not only to determine global parameters of a neutron star, such as mass and radius but also at least theoretically to analyze its internal structure. In general, the construction of a theoretical model of a neutron star requires knowledge of the EoS for a wide range of densities. Typically, different theoretical models are used to describe matter in different density ranges [1–3]. The selection of an appropriate EoS is adequate to the physical conditions prevailing in a given region of a neutron star, whose schematic cross section allows to distinguish its two main parts: the crust and the core. A concise description of neutron star crust must take into account its division into the outer and inner part. The outer crust with density $\rho < 10^6\,\mathrm{g\,cm^{-3}}$ is a region with Coulomb lattice of heavy nuclei being in β equilibrium with relativistic degenerate electron gas [4–6]. The inner crust, being understood as the region whose density is in the range between the neutron drip density ρ_{drip} and the density ρ_t at which the transition to homogeneous nuclear matter occurs, consists of a lattice of neutron-rich nuclei together with a superfluid neutron gas and electron gas. The inner edge of a neutron star's crust in the physical system of a neutron star matter represents the boundary in between the homogeneous matter at high densities and the inhomogeneous one at low densities. Due to the very complex structure of the inner crust, it is a very difficult task to determine this transition density basing on the detailed forms of the equations of state of the nonuniform matter in the crust and matter of the uniform liquid core [7–14]. The neutron drip density ρ_{drip} is quite well known in contrast to the transition density ρ_t, the value of which is highly uncertain. The uncertainty is mainly due to insufficient knowledge of the EoS. This causes the observations of neutron stars to be of special importance as they offer unique opportunities to study properties of dense matter under extreme conditions of density and isospin asymmetry, unattainable in ground-based experiments. Only simultaneous neutron star mass and radius measurements could impose significant constraints on the form of the EoS of neutron star matter, especially in the high-density range. A thorough understanding of the inner structure of a neutron star becomes achievable from the point of view of new possibilities, especially observational ones, the results of which will complement the mass and radius data. One aspect of analyzing the internal structure of a neutron star is understanding the physical properties of its crust. As the crust contains matter with density $\rho < \rho_0$, where ρ_0 is the saturation density, its physical properties can be carried out based on models and methods developed for nuclear physics. The involved theoretical models and results of ground-based experiments are subject to certain uncertainties, translating into uncertainty in determining the crust parameters. This theoretical uncertainty is additionally combined with the uncertainty resulting from astronomical observations. From the observational point of view, new potential limitations on a neutron star's internal structure have to be linked to properly selected phenomena that are of crustal origin [15].

An important parameter characterizing a neutron star's inner structure is the pressure at the crust's inner edge P_t. It was shown that it is directly related to the value of the crustal

*ilona.bednarek@us.edu.pl

fraction of the moment of inertia [16–19]

$$\frac{\Delta I}{I} = \frac{28\pi P_t R^3}{3Mc^2} \times \frac{(1 - 1.67\xi - 0.6\xi^2)}{\xi} \times \left(1 + \frac{2P_t(1 + 5\xi - 14\xi^2)}{\rho_t m c^2 \xi^2}\right)^{-1}, \quad (1)$$

where M and R are neutron star mass and radius, m denotes baryon mass and $\xi = GM/Rc^2$.

Correctly estimating the magnitude of the crustal fraction moment of inertia is a decisive factor that can validate phenomena related to a neutron star's crust region. One of the most important phenomena of this type is pulsar glitching, understood as a sudden increase in a neutron star's rotational frequency resulting from the transfer of angular momentum from the superfluid neutron reservoir to the crust.

For the model to be reliable, it is necessary to estimate the appropriate neutron star crust thickness required to store a sufficient amount of angular momentum to explain large glitches observed in some pulsars. In this case, one expects that a significant fraction of neutron star moment of inertia is related to the superfluid component of the crust [20]. Another way that indirectly allows the crust thickness to be estimated is an observation of neutron stars in X-ray binaries. Accretion of matter from the companion star causes the neutron star crust to heat up and allows for the analysis of its thermal history [21]. In particular, the observation of the binary system KS 1731-260 detected in quiescence [22] indicates the possibility of measuring the cooling timescale of the crust and the total amount of heat stored in it [23]. Considering that theoretical estimates show the dependence of the cooling timescale on the crust thickness, the precise determination of the crust extent allows for the proper understanding of its thermal properties.

There is an analytical estimate of the transition pressure expressed by the properties of nuclear matter. In general, the energy per nucleon of asymmetric nuclear matter $\mathcal{E}(\rho, \delta_a)$ can be represented as a Taylor expansion in asymmetry parameter $\delta_a = (\rho_n - \rho_p)/\rho$, where $\rho = \rho_n + \rho_p$ denotes the baryon density, ρ_n and ρ_p are neutron and proton densities:

$$\mathcal{E}(\rho, \delta_a) = \mathcal{E}(\rho, 0) + E_{\rm sym}(\rho)\delta_a^2. \quad (2)$$

The use of the quadratic polynomial (2)—the parabolic approximation (PA)—in many cases is sufficient to provide a good approximation of the function $\mathcal{E}(\rho, \delta_a)$. The advantage of this approach is the possibility of decomposing the function $\mathcal{E}(\rho, \delta_a)$ into the part that describes the symmetric matter $\mathcal{E}(\rho, 0)$ and the isospin-dependent one. Expansion of functions $\mathcal{E}(\rho, 0)$ and $E_{\rm sym}(\rho)$ into Taylor series around saturation density ρ_0 allows one to write them as follows:

$$\mathcal{E}(\rho, 0) = \mathcal{E}(\rho_0) + \left(\frac{K_0}{2}\right)\left(\frac{\rho - \rho_0}{3\rho_0}\right)^2,$$

$$E_{\rm sym}(\rho) = S_0 + L_0\left(\frac{\rho - \rho_0}{3\rho_0}\right) + \frac{K_{\rm sym,0}}{2}\left(\frac{\rho - \rho_0}{3\rho_0}\right)^2. \quad (3)$$

The analytical form of pressure $P_t \equiv P(\rho_t)$ [18,19] clearly indicates its dependence on the incompressibility K_0 of symmetric nuclear matter and the parameters characterizing its isospin-dependent part—the value of the isospin asymmetry δ_t specified for the transition density ρ_t, symmetry energy $E_{\rm sym}$ and its slope L:

$$P(\rho_t) = \rho_t^2 \frac{K_0}{9\rho_0}\left(\frac{\rho_t - \rho_0}{\rho_0}\right) + \rho_t \delta_t \left(\frac{1 - \delta_t}{2} E_{\rm sym}(\rho_t) + \left(\rho \frac{dE_{\rm sym}}{d\rho}\right)_{\rho_t} \delta_t\right). \quad (4)$$

Since an EoS is a decisive factor determining neutron star properties, it is natural for the existence of correlations between these properties and parameters that characterize the EoS [24]. In the context of the selected, mentioned above observables, correlations with parameters of the EoS and the properties of neutron stars such as the core-core density and pressure, radius, and cooling rate are expected to provide the most information about the structure and properties of the crust. By citing only some of the research results, the conducted analysis showed the existence of correlations with the crust-core transition density and the slope of the symmetry energy at saturation density $L_0 = L(\rho = \rho_0)$ [25,26], transition pressure and the linear combination of the slope L_0 and curvature $K_{\rm sym}$ of the symmetry energy at the subsaturation density $\rho = 0.1$ fm^{-3}, the radii of low mass neutron stars with the symmetry energy slope L_0 [27], and neutron star radii and linear combination of incompressibility K_0 and the slope L_0 [28].

The main source of uncertainty in estimating the crust thickness is insufficient knowledge of the EoS and the values of density and pressure at the crust-core intersection. It has also been shown that the methods used to approximate the form of EoS affect the accuracy of locating the inner edge of the neutron star's crust, i.e., the value of the transition density ρ_t and the corresponding transition pressure P_t [19,29]. One of the reasons for this is that the approximation method used affects symmetry energy [30]. In this paper, an analysis of pressure dispersion based on other factors is presented.

Firstly, the determined pressure dispersion at the core-crust interface results from the fact that one can build the equation based on a whole class of models, not just one particular model in this class. Secondly, under the assumption that the chosen model reasonably well describes properties of neutron star matter and can represent this class of models, allows one to study the influence of all other models from the given class. Consideration, motivated by the actual distribution of star configurations of the entire class of models, allowed one to analyze pressure dispersion based on the mass distribution function of neutron stars. Previously, the analysis of the neutron star mass distribution pointed out that there is a significant signal in the data for the existence of the bimodal distribution of neutron star masses described by the Gaussian mixture model. This mass distribution function also indicates the existence of a sharp cut-off at a maximum neutron star mass, which, if interpreted as the maximum stable neutron star mass, can put constraints on the EoS. This paper aims to quantify the core-crust pressure dispersion. Using the bimodal mass distribution selected in [31] the approximate confidence bands [32] for the pressure, i.e., the confidence intervals over the entire range of neutron star masses were calculated.

II. THE EQUATION OF STATE

The lack of QCD predictions for nuclear systems imposes the continuous development of various theoretical models, which, taking into account the results of existing experimental data would allow for reliable reproduction of atomic nuclei and neutron stars' properties. Concerning systems of such a high degree of complexity, these models offer various modeling scenarios. In general, they can be divided into different classes, one of them being relativistic quantum hadrodynamics (QHD) models. A certain way of grouping these models and distinguishing them based on their parameters is presented in the paper of Dutra *et al.* [33]. This class of models is considered as a type of hierarchical models distinguishable according to parameters determining the EoS. One can write the energy density of these models in a very general form $\mathcal{E}^* \equiv \mathcal{E}^*[\Xi]$, where $\Xi = (\xi_1, \xi_2, \ldots, \xi_d)$ that defines a particular class of models is the vector in d-dimensional parameter space. The function representing the energy density of the ith model belonging to this class has a form $\mathcal{E}_i \equiv \mathcal{E}^*[\Xi_i]$. In this case, vector Ξ_i has k_i nonzero components (for $k_{\min} \leqslant k_i \leqslant d, \xi_k \neq 0$), where $k_{\min}$ is the minimal number of necessary parameters in this model. The maximal model has all components of vector Ξ different from zero. The selected model examined in this paper is denoted with subscript 0 ($\mathcal{E}_0 \equiv \mathcal{E}^*[\Xi_0]$). It lies somewhere in the hierarchy of models. Different variants of individual models contain parameters that determine the coupling between different types of mesons. Examples include self-interactions of scalar mesons, self-interactions of vector mesons, or models with meson cross-terms [33]. Particular models differ in the parameters involved. The archetype of these models, the linear Walecka model, pertains to nucleons interacting through the scalar and vector mesons' exchange. The EoS of asymmetric nuclear matter applied to further analysis performed in this paper is obtained based on a more sophisticated model that considers the extended sector of nonlinear vector and scalar interaction terms. These additional couplings between mesons are indispensable to get results that comply with experimental constraints. In general, a characteristic feature of relativistic models is that they are constructed based on a set of parameters selected to describe both the properties of bulk nuclear matter and finite nuclei correctly. As a result, most models give similar results around saturation density ρ_0. However, their predictions vary considerably at high densities, such as those found inside neutron stars. The choice of the considered model's parametrization (model distinguished by the parametrization Ξ_0) is justified by the necessity to reproduce the properties of nuclear matter and finite nuclei satisfactorily.

The selected saturation properties calculated based on the TM1 model in the case of symmetric nuclear matter are as follows: saturation density $\rho_0 = 0.145$ fm^{-3}, binding energy $E_0(\rho = \rho_0) = -16.26$ MeV, incompressibility $K_0 = 281.3$, $m^\star = m_{\text{eff}}/M = 0.63$. The main properties of the isospin-dependent part are the symmetry energy $E_{\text{sym}} = 36.89$ MeV and its slope $L = 110.79$ MeV. The mixed isoscalar-isovector coupling has been introduced to meet the experimentally acceptable value of the symmetry energy parameters [34–36]. This coupling supplements the isovector part of the model and remodels the symmetry energy dependence on density. It is determined by the combination of parameters Λ_V, g_ρ and is fixed for the symmetry energy $E_{\text{sym}}(\rho) = 25.68$ MeV at the baryon density ρ, which corresponds to the $k_F = 1.15$ fm^{-1}. The TM1 parameter set is presented in Table I [39].

TABLE I. The TM1 parameter set [39] applied in this paper. All meson masses are given in MeV.

σ	$m_\sigma = 511.198$	$g_\sigma = 10.029$	$g_2 = 7.2327\,\text{fm}^{-1}$	$g_3 = 0.6183$
ω	$m_\omega = 783$	$g_\omega = 12.614$	$c_3 = 71.308$	
ρ	$m_\rho = 770$	$g_\rho = 9.2644$		

Interactions in the system can be described by the Lagrangian density function of the form:

$$\mathcal{L}_{\text{int}} = \bar{\psi}\left[g_\sigma\varphi - \left(g_\omega\omega_\mu + \frac{1}{2}g_\rho\boldsymbol{\tau}\cdot\boldsymbol{\rho}_\mu\right)\gamma^\mu\right]\psi - U_{\text{eff}}(\varphi, \omega_\mu, \boldsymbol{\rho}_\mu). \tag{5}$$

This form of Lagrangian density, compared to the archetype of the model, contains additional nonlinear meson interaction terms that are gathered in the function $U_{\text{eff}}(\varphi, \omega_\mu, \boldsymbol{\rho}_\mu)$. Its explicit form is as follows:

$$U_{\text{eff}}(\sigma, \omega, \rho) = \tfrac{1}{3}g_2\sigma^3 + \tfrac{1}{4}g_3\sigma^4 - \tfrac{1}{4}c_3(\omega_\mu\omega^\mu)^2 - \Lambda_V(g_\omega g_\rho)^2(\omega_\mu\omega^\mu)\left(\rho^a_\mu\rho^{a\mu}\right).$$

The field equations calculated for the considered model were solved in the mean-field approximation. In this approach the meson fields operators are replaced by their expectation values: $\sigma \to \langle\sigma\rangle \equiv s$, $\omega_\mu \to \langle\omega_\mu\delta_{\mu 0}\rangle \equiv w$, $\rho^{\mu a} \to \langle\rho^{\mu a}\delta_{0\mu}\delta^{3a}\rangle \equiv r$. This leads to the equations of motion, which have to be solved self-consistently,

$$m_\sigma^2 s + g_2 s^2 + 3s^3 = g_\sigma\rho_s, \tag{6}$$

$$m_\omega^2 w + c_3 w^3 + \Lambda_V(g_\omega g_\rho)^2 r^2 w = g_\omega\rho, \tag{7}$$

$$m_\rho^2 r + \Lambda_V(g_\omega g_\rho)^2 w^2 r = g_\rho\delta_a\rho, \tag{8}$$

$$(i\gamma_\mu\partial^\mu - m_{\text{eff}}(s) - g_\omega\gamma^0 w - g_\rho I_{3N}\gamma^0\tau^3 r)\psi_N = 0. \tag{9}$$

The scalar density ρ_s is given by

$$\rho_s = \sum_{N=n,p}\frac{g_s}{(2\pi)^3}\int_0^{k_{F,N}}\frac{m_{\text{eff}}(s)d^3k}{\sqrt{\left(k^2 + m^2_{\text{eff}}(s)\right)}}, \tag{10}$$

where g_s is the spin-degeneracy factor, $k_{F,N}$ the nucleon Fermi momentum, $k_{F,N} = (6\pi^2/g_s)^{1/3}\rho^{1/3}$, $N = n, p$ (given in units in which $\hbar = c = 1$), and the nucleon effective mass $m_{\text{eff}} = m_N - g_\sigma s$ [40]. The baryon density equals $\rho = \rho_n + \rho_p$. The obtained solutions allow the determination of the energy density $\mathcal{E}_0$ and pressure P of the system:

$$\mathcal{E}_0 = \frac{1}{2}m_\omega^2 w^2 + \frac{1}{2}m_\rho^2 r^2 + \frac{1}{2}m_\sigma^2 s^2 + \frac{3}{4}c_3 w^4 + 3\Lambda_V(g_\omega g_\rho)^2 w^2 r^2 + \frac{1}{3}g_2 s^3 + \frac{1}{4}g_3 s^4 + \sum_{N=n,p}\frac{2}{(2\pi)^3}\int_0^{k_{F,N}} d^3k\sqrt{k^2 + m^2_{\text{eff}}(s)}, \tag{11}$$

$$P = \frac{1}{2}m_\omega^2 w^2 + \frac{1}{2}m_\rho^2 r^2 - \frac{1}{2}m_\sigma^2 s^2 + \frac{1}{4}c_3 w^4 + \Lambda_V (g_\omega g_\rho)^2 w^2 r^2 - \frac{1}{3}g_2 s^3 - \frac{1}{4}g_3 s^4 + \sum_{N=n,p} \frac{2}{3(2\pi)^3}\int_0^{k_{F,N}} d^3k \frac{k^2}{\sqrt{k^2 + m_{\rm eff}^2(s)}}. \quad (12)$$

III. ESTIMATION OF THE VARIANCE OF THE PRESSURE AT THE NEUTRON STAR CORE-CRUST INTERFACE

For a given EoS, which relates the energy density $\mathcal{E}$ to the pressure P, a suitable neutron star model can be obtained by solving the Tolman-Oppenheimer-Volkoff equation representing the general relativistic description of the hydrostatic equilibrium:

$$\frac{dP(r)}{dr} = -\frac{G\mathcal{E}(r)m(r)}{r^2}\left(1+\frac{P(r)}{\mathcal{E}(r)}\right) \times \left(1+\frac{4\pi P(r) r^3}{m(r)}\right)\left(1-\frac{2Gm(r)}{r}\right)^{-1}, \quad (13)$$

$$\frac{dm}{dr} = 4\pi r^2 \mathcal{E}(r). \quad (14)$$

Equation (14) gives the mass enclosed by a sphere of radius r and consequently the total mass of the star can be defined as

$$\mu = m(r=R) = \int_0^R 4\pi\, r^2\, \mathcal{E}(r)\, dr, \quad (15)$$

where R is the star radius. For the performed calculations, the ensemble of neutron stars in the neighborhood of a star with the given mass μ is considered. The mass of a star taken randomly from this ensemble is denoted by μ'. Both stars with masses μ and μ' lie on the $\mu - R$ curve, which has been obtained as a solution of Eq. (13) for a given EoS. The difference in masses $\Delta\mu = \mu' - \mu$, can be represented by the relation

$$\Delta\mu = \mu' - \mu = \int_0^{R'} 4\pi\, r^2\, \mathcal{E}'(r)\, dr - \int_0^R 4\pi\, r^2\, \mathcal{E}(r)\, dr = -\int_0^{R_c+l_c} 4\pi\, r^2\, \delta\mathcal{E}(r)\, dr + \int_{R_c+l_c}^{R_c+l_c'} 4\pi\, r^2\, \mathcal{E}'(r)\, dr + \int_{R_c+l_c'}^{R_c+l_c'+\delta R_c} 4\pi\, r^2\, \mathcal{E}'(r)\, dr = I_1 + I_2 + I_3. \quad (16)$$

In equation (16), R_c and $R_{c'}$ denote the core radius while l and l' denote the crust thickness for both μ and μ' configurations, and the following relations hold $R \equiv R_\mu = R_c + l_c$, $R' \equiv R_{\mu'} = R_c' + l_c'$, $\delta\mathcal{E}(r) = \mathcal{E}(r) - \mathcal{E}'(r)$. The relation

$$\delta R_c = R_c' - R_c \quad (17)$$

allows R' to be expressed as $R' = R_c + \delta R_c + l_c'$.

The energy densities $\mathcal{E}(r)$ and $\mathcal{E}'(r)$ are smooth functions of r both in the core and crust. Thus, it is convenient to write them as the power series:

$$\mathcal{E}(r) = \sum_{k=0}^{\infty} a_k\, r^k, \quad \mathcal{E}'(r) = \sum_{k=0}^{\infty} a_k'\, r^k, \quad (18)$$

separately for the crust and core with the sewing conditions at their interface, i.e., $a_k = a_k^{\rm core}$ for $r \leqslant R_c$ and $a_k = a_k^{\rm crust}$ for $R_c < r \leqslant R$ (and $a_k' = a_k'^{\rm core}$ for $r \leqslant R_c'$ and $a_k' = a_k'^{\rm crust}$ for $R_c' < r \leqslant R'$). Then, all indefinite integrals used in the calculations of integrals in Eq. (16) have the same analytical form and the integrals I_i, $i = 1, 2, 3$ in Eq. (16) resulted as the combinations of following terms

$$Int_a = \frac{4}{3}\pi\, b^3 \sum_{k=0}^{\infty} \frac{3}{k+3} a_k b^k \quad \text{and}$$

$$Int_{a'} = \frac{4}{3}\pi\, b^3 \sum_{k=0}^{\infty} \frac{3}{k+3} a_k' b^k, \quad (19)$$

where b depends on the limit in the particular integral. In the performed numerical calculations both functions $\mathcal{E}(r)$ and $\mathcal{E}'(r)$ have been approximated separately in the core and in the crust by the truncated power series of high enough degree. The mass difference $\Delta\mu$ obtained from Eq. (16) has the form

$$\Delta\mu = \mu' - \mu \approx 4\,\pi (R_c + l_c')^2\, \tilde{\mathcal{E}}_c\, \delta R_c + I_{\mu'\mu}\,, \quad (20)$$

where $I_{\mu'\mu} = I_1 + I_2$. Expanding I_3 to the first power of δR_c leads to the equation,

$$\frac{I_3}{4\,\pi (R_c + l_c')^2} \approx \tilde{\mathcal{E}}_c\, \delta R_c = \mathcal{E}'(r = R_c + l_c')\, \delta R_c = \left(\sum_{k=0}^{\infty} a_k' (R_c + l_c')^k\right) \delta R_c, \quad (21)$$

where $\tilde{\mathcal{E}}_c = \mathcal{E}'(r = R_c + l_c')$.

The estimator of the pressure variance $\sigma^2(P_t)$ at the core-crust interface is constructed below. The estimation is based on the model of EoS selected from the given class of models $E^*(\Xi)$. This chosen model (with index "0") is proposed as an approximation to the true one in the same sense that the type II regression function approximates the type I regression function, which is the truly unknown. That means the pressure $P_{t,0}$ at the core-crust interface in the given model (with the energy density denoted by $\mathcal{E}_0$) approximates the expectation value [37], i.e., $P_{t,0} \approx E(P_t)$.

While $P_{t,0}$ is proposed as the approximation of $E(P_t)$, the variance $\widehat{\sigma^2}(P_t)$ constructed in this paper is the model-based estimator of the true variance $\sigma^2(P_t)$ [37]. It will be shown that $\widehat{\sigma^2}(P_t)$ depends on μ.

Each mass μ' distinguishes a subpopulation of neutron stars with this mass value. The functions $\mathcal{E}_i(r)$ that represents the radial dependence of the energy density for each ith model (Sec. II) are solutions obtained for configurations with different masses μ', based on theoretical models belonging to the considered class of models. The chosen model "0" leads to the solution $\mathcal{E}_0(r)$. One can assume that each of the functions $\mathcal{E}_i(r)$ could be written as follows:

$$\mathcal{E}_i(r) = \mathcal{E}_0(r) + \delta\mathcal{E}_i(r), \quad (22)$$

where $\delta\mathcal{E}_i(r)$ denotes the differences in energy of each ith model that belongs to $\mathcal{E}^*[\Xi]$ and $\mathcal{E}_0(r)$. The Taylor expansion of the function $\mathcal{E}_i(r)$ around $R_c = R_c(\mu)$, which denotes the core radius calculated based on model "0" for the configuration with mass μ leads to the following relation:

$$\mathcal{E}_i(r) = \mathcal{E}_0(R_c) + \delta\mathcal{E}_i(R_c) + \frac{d\mathcal{E}_0(r)}{dr}|_{r=R_c}(r - R_c) + \frac{d\delta\mathcal{E}_i(r)}{dr}|_{r=R_c}(r - R_c) + \dots. \tag{23}$$

For $r = R_c'$ this equation reads

$$\mathcal{E}_i(R_c') = \mathcal{E}_0(R_c) + \delta\mathcal{E}_i(R_c) + \frac{d\mathcal{E}_0(r)}{dr}|_{r=R_c}(R_c' - R_c) + \frac{d\delta\mathcal{E}_i(r)}{dr}|_{r=R_c}(R_c' - R_c) + \dots. \tag{24}$$

Considering models $\mathcal{E}_i$ that belong to the $E^*(\Xi)$ class, the pointwise mean of all different models (i.e., in $r = R_c'$) can be determined. Then, the assumption that $\mathcal{E}_0(r)$ gives the solid estimation of the true unknown energy density function means that

$$\overline{\mathcal{E}_i(r)} = \mathcal{E}_0(r), \quad \overline{\delta\mathcal{E}_i(r)} = 0, \quad \overline{\frac{d\delta\mathcal{E}_i(r)}{dr}} = 0. \tag{25}$$

From Eq. (24) stems that the difference $\Delta\mathcal{E}$ between the value $\overline{\mathcal{E}_i(R_c')} = \mathcal{E}_0(R_c')$ and $\mathcal{E}_0(R_c)$ that is calculated at R_c for μ-mass configuration, is equal to

$$\Delta\mathcal{E} = \overline{\mathcal{E}_i(R_c')} - \mathcal{E}_0(R_c) = \mathcal{E}_0(R_c') - \mathcal{E}_0(R_c) = \frac{d\mathcal{E}_0(r)}{dr}|_{r=R_c}\delta R_c + \dots, \tag{26}$$

where $\delta R_c = R_c' - R_c$. When $\mathcal{E}$ in Eqs. (16)–(21) is given by $\mathcal{E}_0$ then δR_c, Eq. (17), can be determined from Eq. (20). Then, the expansion (26) written to the second order in δR_c reads

$$\Delta\mathcal{E} = \frac{d\mathcal{E}}{dr}|_{R_c}\delta R_c + \frac{1}{2}\frac{d^2\mathcal{E}}{dr^2}|_{R_c}(\delta R_c)^2 + \dots = \frac{d\mathcal{E}}{dr}|_{R_c}\frac{\widetilde{\Delta\mu}}{4\pi(R_c + l_c')^2\tilde{\mathcal{E}}_c} + \frac{1}{2}\frac{d^2\mathcal{E}}{dr^2}|_{R_c}\left(\frac{\widetilde{\Delta\mu}}{4\pi(R_c + l_c')^2\tilde{\mathcal{E}}_c}\right)^2 + \dots, \tag{27}$$

where in the second line the relation (20)

$$\widetilde{\Delta\mu} = \Delta\mu - I_{\mu'\mu} = \mu' - \tilde{\mu} \tag{28}$$

has been used with $\tilde{\mu} := \mu + I_{\mu'\mu}$. Squaring Eq. (27) gives

$$(\Delta\mathcal{E})^2 = \left(\frac{d\mathcal{E}}{dr}|_{R_c}\right)^2\left(\frac{\widetilde{\Delta\mu}}{4\pi(R_c + l_c')^2\tilde{\mathcal{E}}_c}\right)^2 + \frac{d\mathcal{E}}{dr}|_{R_c}\frac{d^2\mathcal{E}}{dr^2}|_{R_c}\left(\frac{\widetilde{\Delta\mu}}{4\pi(R_c + l_c')^2\tilde{\mathcal{E}}_c}\right)^3 + \frac{1}{4}\left(\frac{d^2\mathcal{E}}{dr^2}|_{R_c}\right)^2\left(\frac{\widetilde{\Delta\mu}}{4\pi(R_c + l_c')^2\tilde{\mathcal{E}}_c}\right)^4 + \dots. \tag{29}$$

The values of higher-order terms are roughly of an order of magnitude lower then the linear term and in further analysis, only the linear term is kept in Eq. (29).

The Taylor expansion of the pressure function $P(\mathcal{E}_i(r))$ around $\mathcal{E}(R_c)$ in the P_t dispersion analysis gives for the means, i.e., as the consequence of (26), the equality

$$P_t \equiv P(\overline{\mathcal{E}_i(R_c')}) = P(\mathcal{E})|_{R_c'} = P_{t,0} + \frac{dP}{d\mathcal{E}}|_{\mathcal{E}(R_c)}\Delta\mathcal{E}, \tag{30}$$

where $P_{t,0} = P(\mathcal{E}(R_c))$. This gives the mean variation taken over all $\mathcal{E}_i$ models at the core-crust interface of a neutron star with the mass μ:

$$\Delta P_t = P_t - P_{t,0} = \frac{dP}{d\mathcal{E}}|_{\mathcal{E}(R_c)}\Delta\mathcal{E}. \tag{31}$$

The aim of this paper is to calculate the variance $\widehat{\sigma^2}(P_t) = \widehat{E}\{(\Delta P_t)^2\}$ [37], for the discussed ensemble of neutron stars. The mean $\widehat{E}\{(\Delta P_t)^2\}$ is taken over all stars of mass μ'. Basing on the results from Eq. (29), the pressure variance for the star with the fixed mass μ can be obtained:

$$\sigma_{P_t}^2 \equiv \widehat{\sigma^2}(P_t) = \widehat{E}\left[(\Delta P_t)^2\right] = \widehat{E}\left[\left(\frac{dP}{d\mathcal{E}}|_{\mathcal{E}(R_c)}\right)^2(\Delta\mathcal{E})^2\right] = \widehat{E}\left[\left(\frac{dP}{d\mathcal{E}}|_{\mathcal{E}(R_c)}\right)^2\left(\frac{d\mathcal{E}}{dr}|_{R_c}\right)^2 \times \left(\frac{1}{4\pi(R_c + l_c')^2\tilde{\mathcal{E}}_c}\right)^2(\widetilde{\Delta\mu})^2\right]. \tag{32}$$

Using the chain rule,

$$\left(\frac{dP}{dr}|_{R_c}\right)^2 = \left(\frac{dP}{d\mathcal{E}}|_{\mathcal{E}(R_c)}\right)^2\left(\frac{d\mathcal{E}}{dr}|_{R_c}\right)^2, \tag{33}$$

and neglecting the terms proportional to P/c^2 in Eq. (13) allows for adopting a given approximation [38]:

$$\frac{dP}{dr}|_{R_c} = -\frac{M}{R_c^2}\frac{\mathcal{E}}{1 - \frac{r_g}{R_c}}, \tag{34}$$

and thus Eq. (32) takes the following form:

$$\sigma_{P_t}^2 = \widehat{E}\left[\left(-\frac{\mu}{R_c^2}\frac{\mathcal{E}(R_c)}{1 - \frac{r_g}{R_c}}\right)^2\left(\frac{1}{4\pi(R_c + l_c')^2\tilde{\mathcal{E}}_c}\right)^2(\widetilde{\Delta\mu})^2\right]. \tag{35}$$

Computing the pressure variance (32) requires knowledge of the mass μ' distribution. The model selection analyzes for the set of n-component mixture models described by:

$$p(\mu'|\theta) = \sum_{i=1}^{n} r_i\,\mathcal{N}(\mu'|\bar{\mu}_i, \sigma_i)\,\Theta(\mu' - \mu'_{\max})/\Phi_i \tag{36}$$

was performed in [31]. Here, $\theta = \{(\bar{\mu}_i)_{i=1}^n, (\sigma_i)_{i=1}^n, (r_i)_{i=1}^n, \mu'_{\max}\}$ and $\bar{\mu}_i, \sigma_i$, and r_i are the mean, standard deviation, and relative weight of the ith Gaussian component, respectively, $i = 1, 2, \dots n$. $\mathcal{N}$ denotes the Gaussian density and Θ is the Heaviside function.

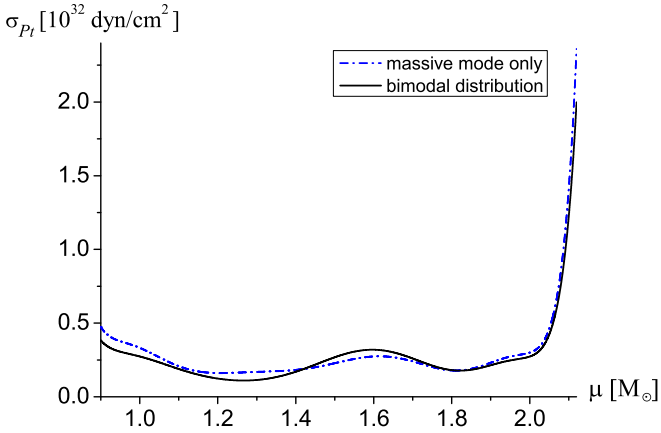

FIG. 1. The dependence of the standard deviation σ_{P_t} of the transition pressure on the mass μ. The comparison of the results obtained for the heavy mode only vs bimodal distribution is given. Only in the vicinity of the minimum of σ_{P_t}, the results obtained for both types of neutron mass distributions are similar. Better visualization of the effect of the distribution type in this vicinity is given in Fig. 2.

The normalization constants $\Phi_i \equiv \Phi(\bar{\mu}_i, \sigma_i; \mu'_{\min}, \mu'_{\max})$ are integrals over the Gaussian components (which take into account the allowed NS mass range):

$$\Phi(\bar{\mu}, \sigma; \mu'_{\min}, \mu'_{\max}) = \int_{\mu'_{\min}}^{\mu'_{\max}} \mathcal{N}(x|\bar{\mu}, \sigma)\, dx \qquad (37)$$

and the normalization of the distribution requires that $\sum_{i=1}^{n} r_i = 1$. In [31], the minimal mass taken into account is equal to $\mu'_{\min} = 0.9\ \mathrm{M}_\odot$ and the $n = 2$ components Gaussian mixture model with a cut-off at $\mu'_{\max}$ was selected. This model has the following estimates of parameters (only mean values are quoted) [31]: $n = 2$ components, $\mu'_{\max} < 2.9\ \mathrm{M}_\odot$, $\bar{\mu}_1 = 1.34\ \mathrm{M}_\odot$, $\bar{\mu}_2 = 1.80\ \mathrm{M}_\odot$, $\sigma_1 = 0.07$, $\sigma_2 = 0.21$, $r_1 = 0.65$, $\mu'_{\max} = \mu_{\max} = 2.12\ \mathrm{M}_\odot$.

To calculate $\sigma^2(P_t)$ for each particular value of μ, the distribution of the square of the deviation of pressure P_t from the pressure $P_{t,0}$,

$$(\Delta P_t)^2 = \left(-\frac{\mu}{R_c^2}\frac{\mathcal{E}(R_c)}{1-\frac{r_g}{R_c}}\right)^2 \left(\frac{1}{4\pi\,(R_c + l'_c)^2 \tilde{\mathcal{E}}_c}\right)^2 (\widetilde{\Delta\mu})^2, \qquad (38)$$

had to be generated numerically from the distribution of μ' given by Eq. (36). The results correspond to the pressure dispersion at the core-crust interface due to the inclusion of neutron star configurations calculated based on other models from the $\mathcal{E}^*[\Xi]$ class of models. The dependence of the standard deviation $\sigma_{P_t} := \sqrt{\widehat{\sigma^2}(P_t)}$, Eq. (32), on the mass μ is presented in Fig. 1. This figure shows the existence of two minima, the shallow one at $\mu = 1.21\ \mathrm{M}_\odot$ with $\sigma_{P_t} \approx 1.6 \times 10^{31}\ \mathrm{dyn\,cm^{-2}}$, and the other one at $\mu = 1.81\ \mathrm{M}_\odot$ with $\sigma_{P_t} \approx 1.78 \times 10^{31}\ \mathrm{dyn\,cm^{-2}}$. The standard deviations for two stellar configurations: for $\mu = \bar{\mu}_1 = 1.34\ \mathrm{M}_\odot$, i.e., for the maximum of neutron star lower mass mode distribution, and for $\mu = \bar{\mu}_2 = 1.8\ \mathrm{M}_\odot$, i.e., for the maximum of neutron star higher mass mode distribution, are given in Table II. To better

TABLE II. The standard deviation σ_{P_t} for the chosen stellar configurations with mass μ.

μ	σ_{P_t}
$\bar{\mu}_1 = 1.34\ \mathrm{M}_\odot$	$1.75 \times 10^{31}\ \mathrm{dyn\,cm^{-2}}$
$\bar{\mu}_2 = 1.8\ \mathrm{M}_\odot$	$1.79 \times 10^{31}\ \mathrm{dyn\,cm^{-2}}$

visualize the impact of the type of neutron star mass distribution on the dispersion of P_t, the function of σ_{P_t} on μ in the interval $\bar{\mu}_2 \pm \sigma_2 = (1.59, 2.01) \times\ \mathrm{M}_\odot$, i.e., around the maximum of the neutron star heavy mode mass distribution, is presented in Fig. 2. This figure comprises the results obtained for the heavy mode only versus bimodal distribution. It shows that only in the vicinity of the minimum of σ_{P_t}, the results obtained for both types of neutron mass distributions are similar. The analysis also shows that the quality of the P_t estimation at the core-crust interface deteriorates rapidly for neutron star masses, which are greater than $\sim 2.02\ \mathrm{M}_\odot$. This is illustrated in Fig. 1 and Fig. 3. Eq. (35) implies that the factor $1 - \frac{r_g}{R_c}$ in the denominator is one of the sources of the deterioration of the accuracy in finding the variance of pressure for the heaviest stellar configurations. When changing the mass from $\mu = 0.9\ \mathrm{M}_\odot$ to $\mu_{\max} = 2.12\ \mathrm{M}_\odot$, this factor diminishes about twice. In Fig. 3 the dependence of the relative dispersion $\sigma_{P_t}/P_{t,0}$ on the neutron star mass μ is plotted. Using Eq. (38) and the distribution of μ' given by Eq. (36), the distribution of ΔP_t for each particular mass μ was obtained. This enables obtaining the probability $\mathcal{P}_{\sigma_{P_t}} \equiv \mathcal{P}(P_{t,0} - \sigma_{P_t} < P_t < P_{t,0} + \sigma_{P_t})$ for each mass μ. The dependence of the probability $\mathcal{P}_{\sigma_{P_t}}$ on neutron star mass μ is depicted in Fig. 4. Having $\mathcal{P}_{\sigma_{P_t}}$ for each μ, the confidence bands $P_{t,0} \pm \sigma_{P_t}$ [32], for the core-crust interface pressure, presented in Fig. 5, gains the probabilistic meaning. It means, assuming that the considered theoretical model of the neutron star indexed by 0 is the solid one and the μ' mass distribution (36) is correct, that the percentage of stars of mass μ with P_t falling into the range $(P_{t,0} - \sigma_{P_t} <$

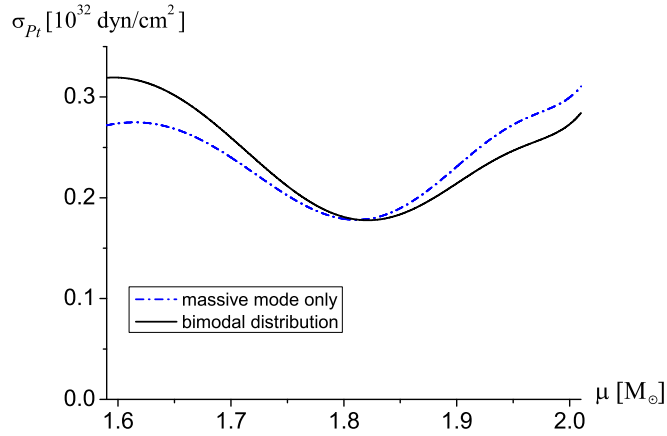

FIG. 2. The dependence of the standard deviation σ_{P_t} of the transition pressure at the core-crust interface on the mass μ for the mass range $\bar{\mu}_2 \pm \sigma_2 = (1.59, 2.01) \times\ \mathrm{M}_\odot$ is shown. The results were obtained for both the bimodal distribution function and the heavy mode alone.

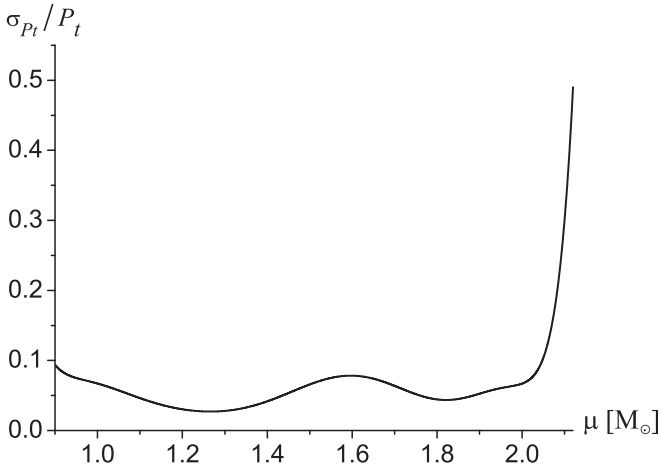

FIG. 3. The dependence of the relative standard deviation $\sigma_{P_t}/P_{t,0}$ calculated at the core-crust interface on the mass μ. The bigger the value of $\sigma_{P_t}/P_{t,0}$, the worse is the quality of the pressure P_t estimation. The calculations were performed for the bimodal distribution function.

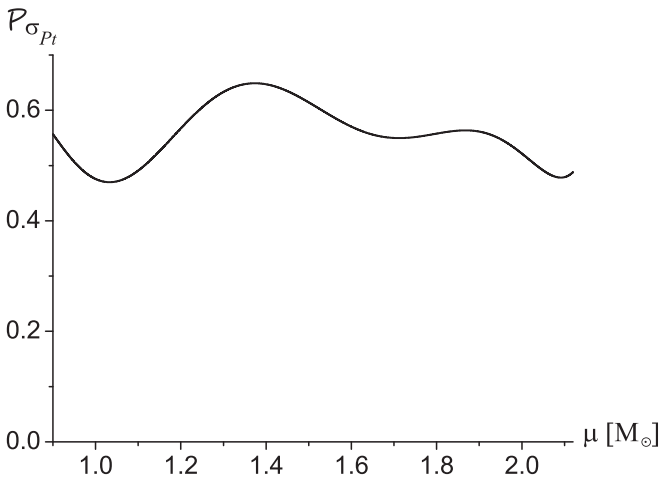

FIG. 4. The dependence of the probability $\mathcal{P}_{\sigma_{P_t}} \equiv \mathcal{P}(P_{t,0} - \sigma_{P_t} < P_t < P_{t,0} - \sigma_{P_t})$ on the mass μ. The calculations were performed for the bimodal distribution function.

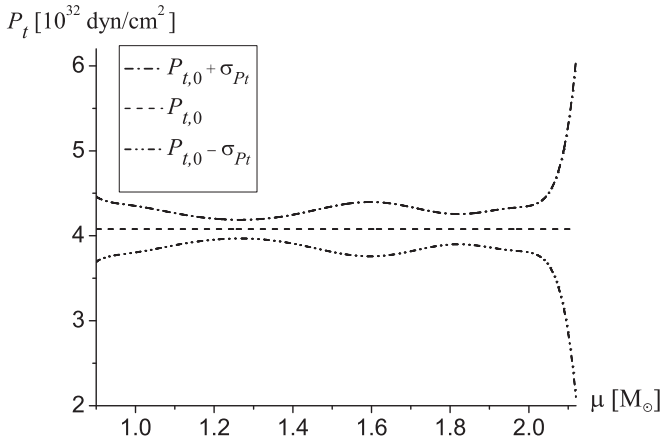

FIG. 5. The confidence bands $P_{t,0} \pm \sigma_{P_t}$ for the pressure P_t at the core-crust interface calculated for the bimodal distribution function.

$P_t < P_{t,0} + \sigma_{P_t}$) should be around $\mathcal{P}_{\sigma_{P_t}} \times 100\%$ for a large sample. At the same time, the probability of a finding of any particular physical μ-mass star configuration with the core-crust pressure $P_t \leqslant P_{t,0} - \sigma_{P_t}$ or $P_t \geqslant P_{t,0} + \sigma_{P_t}$ should be around $1 - \mathcal{P}_{\sigma_{P_t}}$ [42].

Finally, there are two sources of errors in the calculation of $\sigma^2_{P_t}$ given by Eq. (35), the theoretical and numerical ones. The main theoretical error arises from neglecting higher-order terms in Eq. (29) that leads on average to approximately 10% error in the calculation of $(\Delta\mathcal{E})^2$. This average denotes the arithmetic mean over the μ masses. The numerical error is connected with the fact that in calculations the expectation value in Eq. (35) was replaced by the mean over the finite number of star configuration masses μ'. On average (in the μ masses) this gives the mean numerical error equal approximately to 5%. The theoretical and numerical errors contribute to the error of $\sigma^2_{P_t}$ in Eq. (35) independently and therefore the total error given by the Pythagorean formula is of the order of $(\sqrt{0.1^2 + 0.05^2})100\% \approx 11\%$. Likewise the error in the estimation of the probability $\mathcal{P}_{\sigma_{P_t}} \equiv \mathcal{P}(P_{t,0} - \sigma_{P_t} < P_t < P_{t,0} - \sigma_{P_t})$ depicted in Fig. 4 is on average (in the μ masses) equal approximately to 11%.

IV. CONCLUSIONS

In this paper, a method of determining the variance $\sigma^2_{P_t} \equiv \widehat{\sigma^2}(P_t)$ of pressure P_t at the core-crust interference was developed. Using the model of the EoS selected in Sec. III the P_t pressure dispersion σ_{P_t} at the core-crust interface was reconstructed based firstly on the class of EoS models that includes the TM1 model and secondly on the observed neutron star mass distribution function given by Eq. (36). In the next step, the probability $\mathcal{P}_{\sigma_{P_t}}$ of finding of the particular μ-mass star configuration with the core-crust pressure $P_{t,0} - \sigma_{P_t} < P_t < P_{t,0} + \sigma_{P_t}$, was determined. This enabled the interval estimation of the value of pressure P_t as a function of neutron star mass μ, i.e., the confidence bands $P_{t,0} \pm \sigma_{P_t}$ were constructed. The conducted analysis allows us to conclude that the obtained results depend on the neutron star mass μ. The least accuracy in determining the pressure P_t is obtained for the heaviest stellar configuration. It was noted that one of the factors that influences the quality of the transition pressure determination is the neutron star mass distribution function.

As the transition pressure P_t is model dependent, the performed analysis also offers tools for comparing different theoretical models that describe neutron star matter and evaluating models within given class of models to obtain the best quality of transition pressure determination.

The proposed method makes it possible to examine how the dispersion of the transition pressure P_t may be sensitive to changes in factors that have been used in the calculations performed, with the most important one being the selected model of the EoS. By carrying out a similar analysis for different models within a given class of models or different model classes, it can be estimated which theoretical model gives the lowest uncertainty in the determination of the pressure P_t. This enables one to compare the constructed confidence bands for observable quantities with the observations. In that

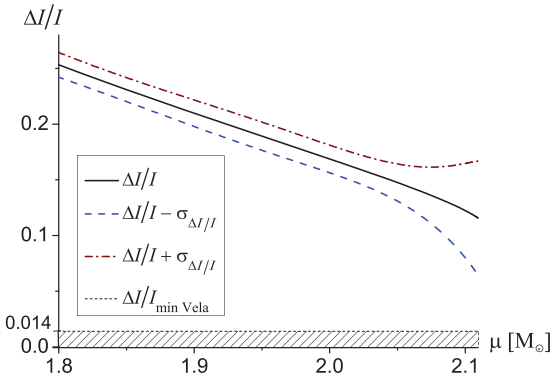

FIG. 6. The confidence bands $\Delta I/I \pm \sigma_{\Delta I/I}$ for the crustal fraction of the moment of inertia $\Delta I/I$ calculated for the bimodal distribution function, for the selected model; results are given by the solid line. $\Delta I/I_{\text{min Vela}}$ denotes the lower limit of the possible experimentally acceptable values of $\Delta I/I$ from the Vela pulsar. The dashed area is the one that is excluded by the constraints obtained for the Vela pulsar.

way, knowledge of the uncertainty resulting from the used theoretical model influences the interpretation of neutron star observational parameters.

The presented method is designed for general application in estimating uncertainties in determining neutron star properties that depend on the transition pressure P_t. The crustal fraction of the moment of inertia $\Delta I/I$ is of particular relevance in this paper as it depends directly on the transition pressure. The results can be related to the known experimental constraint on the crustal fraction of the moment of inertia obtained from studying the glitches of the Vela pulsar [41]. Within a given class of models and for models close to the selected one under the assumption of linear approximation in P_t of Eq. (1) the following formula can be derived [42]:

$$\sigma_{\Delta I/I} = \left(\frac{28\pi R^3}{3Mc^2}\right) \times \left|\frac{1 - 1.67\xi - 0.6\xi^2}{\xi}\right| \sigma_{Pt}. \tag{39}$$

This approximation can be obtained considering that the ratio of the pressure to energy density at the crustal region is a small quantity [43]. As for applying the proposed method, the approximate determination of the $\pm 1\sigma_{\Delta I/I}$ confidence bands for the $\Delta I/I$ is presented. The results obtained for neutron stars in a given mass range, which includes the mass of the Vela pulsar [44], are shown in Fig. 6. The dashed area is the one that is excluded by the constraints obtained for the Vela pulsar. The points that lie between the confidence bands satisfy the $\Delta I/I$ constraint and thus from this figure it can be seen that at the $1 - \mathcal{P}_{\sigma_{Pt}}$ significance level [42] there is no reason to reject the hypothesis that $\Delta I/I$ for the Vela pulsar is described by the selected model. The very low value of $\Delta I/I$ for the Vela pulsar is the reason why this limitation is met over the entire mass range. By finding dependence or correlations between transition pressure and observational parameters, one can control the uncertainty resulting from the theoretical model describing the star. Namely, the P_t dispersion allows to be transferred to the estimated dispersion of the internal structure of the star. Thus, as the uncertainty in determining the pressure value P_t at the core-crust interface is transferred to the uncertainty in determining the position of the inner edge of the crust, it also influences the precision of determining the thickness of the crust. As it was presented above, the transition pressure determined at the inner edge of a neutron star crust relates closely to the crustal fraction of the moment of inertia, which can be constrained based on observations of pulsar glitches. Knowing the moment of inertia of the crust is necessary to estimate its thickness correctly. This allows one to hope that theoretical calculations combined with the observation effort will yield insight into the structure of neutron stars.

[1] S. L. Shapiro and S. A. Teukolsky, *Black Holes, White Dwarfs, and Neutron Stars* (Wiley Interscience, New York, 2004).

[2] P. Haensel, A. Y. Potekhin, and D. G. Yakovlev, *Neutron Stars 1: Equation of State and Structure*, Astrophysics and Space Science Library, Vol. 326 (Springer, New York, 2007).

[3] F. Ji, J. Hu, S. Bao, and H. Shen, Phys. Rev. C **100**, 045801 (2019).

[4] G. Baym, C. J. Pethick, and P. Sutherland, Astrophys. J. **170**, 299 (1971).

[5] P. Haensel and B. Pichon, Astron. Astrophys. **283**, 313 (1994).

[6] S. B. Ruster, M. Hempel, and J. Schaffner-Bielich, Phys. Rev. C **73**, 035804 (2006).

[7] C. J. Horowitz, M. A. Perez-Garcia, and J. Piekarewicz, Phys. Rev. C **69**, 045804 (2004).

[8] C. J. Horowitz, M. A. Perez-Garcia, D. K. Berry, and J. Piekarewicz, Phys. Rev. C **72**, 035801 (2005).

[9] T. Maruyama, T. Tatsumi, D. N. Voskresensky, T. Tanigawa, and S. Chiba, Phys. Rev. C **72**, 015802 (2005).

[10] H. Sonoda, G. Watanabe, K. Sato, K. Yasuoka, and T. Ebisuzaki, Phys. Rev. C **77**, 035806 (2008).

[11] G. Watanabe, H. Sonoda, T. Maruyama, K. Sato, K. Yasuoka, and T. Ebisuzaki, Phys. Rev. Lett. **103**, 121101 (2009).

[12] S. S. Avancini, D. P. Menezes, M. D. Alloy, J. R. Marinelli, M. M. W. Moraes, and C. Providencia, Phys. Rev. C **78**, 015802 (2008).

[13] S. S. Avancini, L. Brito, J. R. Marinelli, D. P. Menezes, M. M. W. de Moraes, C. Providência, and A. M. Santos, Phys. Rev. C **79**, 035804 (2009).

[14] S. S. Avancini, S. Chiacchiera, D. P. Menezes, and C. Providência, Phys. Rev. C **82**, 055807 (2010).

[15] N. Chamel and P. Haensel, Living Rev. Relativ. **11**, 10 (2008).

[16] J. M. Lattimer and M. Prakash, Phys. Rep. **333**, 121 (2000).

[17] J. M. Lattimer and M. Prakash, Astrophys. J. **550**, 426 (2001).

[18] J. M. Lattimer and M. Prakash, Phys. Rep. **442**, 109 (2007).

[19] J. Xu, L.-W. Chen, B.-A. Li, and H.-R. Ma, Astrophys. J. **697**, 1549 (2009).
[20] A. W. Steiner, S. Gandolfi, and F. J. Fattoyev, and W. G. Newton, Phys. Rev. C **91**, 015804 (2015).
[21] E. F. Brown and A. Cumming, Astrophys. J. **698**, 1020 (2009).
[22] R. E. Rutledge, L. Bildsten, E. F. Brown, G. G. Pavlov, V. E. Zavlin, and G. Ushomirsky, Astrophys. J. **580**, 413 (2002).
[23] D. Page and S. Reddy, Phys. Rev. Lett. **111**, 241102 (2013).
[24] I. Bednarek, J. Sładkowski, and J. Syska, Nucl. Phys., A. **997**, 121727 (2020).
[25] C. Ducoin, J. Margueron, and C. Providencia, Europhys. Lett. **91**, 32001 (2010).
[26] W. G. Newton, M. Gearheart, and B.-A. Li, Astrophys. J. Suppl. **204**, 9 (2013).
[27] F. J. Fattoyev and J. Piekarewicz, Phys. Rev. C **86**, 015802 (2012).
[28] N. Alam, B. K. Agrawal, M. Fortin, H. Pais, C. Providencia, Ad. R. Raduta, and A. Sulaksono, Phys. Rev. C **94**, 052801(R) (2016).
[29] I. Bednarek, J. Sładkowski, and J. Syska, J. Phys. Soc. Jpn. **88**, 124201 (2019).
[30] I. Bednarek, J. Sładkowski, and J. Syska, Symmetry **12**, 898 (2020).
[31] J. Alsing, H. O. Siva, and E. Berti, Mon. Not. R. Astron. Soc. **478**, 1377 (2018).
[32] W. Liu, *Simultaneous Inference in Regression* (CRC Press, Boca Raton, 2010).
[33] M. Dutra, O. Lourenco, S. S. Avancini, B. V. Carlson, A. Delfino, D. P. Menezes, C. Providencia, S. Typel, and J. R. Stone, Phys. Rev. C **90**, 055203 (2014).
[34] C. J. Horowitz and J. Piekarewicz, Phys. Rev. Lett. **86**, 5647 (2001).
[35] B. K. Sharma and S. Pal, Phys. Lett. B **682**, 23 (2009).
[36] I. Bednarek and M. Pienkos, Acta Phys. Pol. B **46**, 2343 (2015).
[37] D. C. Montgomery and G. C. Runger, *Applied Statistics and Probability for Engineers*, 3rd edition (John Wiley & Sons, Inc., New York, 2003).
[38] J. L. Zdunik, M. Fortin, and P. Haensel, Astron. Astrophys. **599**, A119 (2017).
[39] Y. Sugahara and H. Toki, Nucl. Phys. A **579**, 557 (1994).
[40] I. Bednarek, R. Manka, and M. Pienkos, PLoS One **9**, e106368 (2014).
[41] B. Link, R. I. Epstein, and J. M. Lattimer, Phys. Rev. Lett. **83**, 3362 (1999).
[42] L. Lista, *Statistical Methods for Data Analysis in Particle Physics*, 2nd edition (Springer, New York, 2017).
[43] J. Piekarewicz, F. J. Fattoyev, and C. J. Horowitz, Phys. Rev. C **90**, 015803 (2014).
[44] M. Falanga, E. Bozzo, A. Lutovinov, J. Bonnet-Bidaud, Y. Fetisova, and J. Puls, Astron. Astrophys. **577**, A130 (2015).